Vascular disease-causing mutation, smooth muscle α-actin R258C, dominantly suppresses functions of α-actin in human patient fibroblasts

Zhenan Liu[a], Audrey N. Chang[a], Frederick Grinnell[b], Kathleen M. Trybus[c], Dianna M. Milewicz[d], James T. Stull[a], and Kristine E. Kamm[a,1]

[a]Department of Physiology, University of Texas Southwestern Medical Center, Dallas, TX 75390; [b]Department of Cell Biology, University of Texas Southwestern Medical Center, Dallas, TX 75390; [c]Department of Molecular Physiology and Biophysics, University of Vermont, Burlington, VT 05446; and [d]Department of Internal Medicine, University of Texas Health Science Center, Houston, TX 77030

Edited by Edward D. Korn, National Heart, Lung, and Blood Institute, Bethesda, MD, and approved June 1, 2017 (received for review March 2, 2017)

The most common genetic alterations for familial thoracic aortic aneurysms and dissections (TAAD) are missense mutations in vascular smooth muscle (SM) α-actin encoded by *ACTA2*. We focus here on *ACTA2*–R258C, a recurrent mutation associated with early onset of TAAD and occlusive moyamoya-like cerebrovascular disease. Recent biochemical results with SM α-actin–R258C predicted that this variant will compromise multiple actin-dependent functions in intact cells and tissues, but a model system to measure R258C-induced effects was lacking. We describe the development of an approach to interrogate functional consequences of actin mutations in affected patient-derived cells. Primary dermal fibroblasts from R258C patients exhibited increased proliferative capacity compared with controls, consistent with inhibition of growth suppression attributed to SM α-actin. Telomerase-immortalized lines of control and R258C human dermal fibroblasts were established and SM α-actin expression induced with adenovirus encoding myocardin-related transcription factor A, a potent coactivator of *ACTA2*. Two-dimensional Western blotting confirmed induction of both wild-type and mutant SM α-actin in heterozygous *ACTA2*–R258C cells. Expression of mutant SM α-actin in heterozygous *ACTA2*–R258C fibroblasts abrogated the significant effects of SM α-actin induction on formation of stress fibers and focal adhesions, filamentous to soluble actin ratio, matrix contraction, and cell migration. These results demonstrate that R258C dominantly disrupts cytoskeletal functions attributed to SM α-actin in fibroblasts and are consistent with deficiencies in multiple cytoskeletal functions. Thus, cellular defects due to this *ACTA2* mutation in both aortic smooth muscle cells and adventitial fibroblasts may contribute to development of TAAD and proliferative occlusive vascular disease.

thoracic aortic aneurysms | ACTA2 mutation | vascular disease | cell migration | human fibroblasts

Aortic aneurysm disease ranks consistently in the top 20 most common causes of death in the United States (1). The natural history of an aneurysm in the thoracic aortic root or ascending aorta is progressive, asymptomatic enlargement over time that can lead to an acute, frequently lethal, dissection in the absence of surgical repair (2–4). Approximately 25% of patients with thoracic aortic aneurysms and dissections (TAADs) have a single gene mutation predisposing to this disease in an autosomal dominant pattern. Affected genes encode proteins involved in smooth muscle (SM) contraction or structural components of the elastic matrix that comprise the contractile-elastic unit (5). Mutations in the *ACTA2* gene, encoding the SM-specific isoform of α-actin (SM α-actin), are the major cause of familial TAAD, responsible for disease in 12–21% of these families (6, 7). Over 40 mutations in *ACTA2* have been identified leading to a high overall cumulative risk of an aortic event, and specific mutations, including R258C, are associated with significantly greater risk (6). Intriguingly, several *ACTA2* mutations, including R258C, predispose to occlusive vascular diseases, potentially arising in part from increased smooth muscle cell proliferation and migration in small, muscular arteries that can lead to stroke or myocardial infarction (7, 8).

SM α-actin is expressed in abundance in vascular smooth muscle, comprising 50–70% of total actin, with the remainder composed of β-cytoplasmic and γ-actins (9–11). Whereas SM α-actin expression is normally restricted to smooth muscle cells, it can also be expressed in nonmuscle cells, most notably myofibroblasts that use cell traction forces to remodel extracellular matrix (12). Filamentous actin (F-actin) arises from the polymerization of monomeric globular actin (G-actin). F-actin supports force production through its interaction with myosin filaments, and it supports force transmission via the actin cytoskeleton that stabilizes adhesive structures connected to the elastin-extracellular matrix (13). Dissected aortas exhibit characteristic features, including loss and disarray of smooth muscle cells in the medial layer, loss of elastic fibers, and proteoglycan accumulation in the medial space (4). These observations have led to the hypothesis that TAADs arise because of inappropriate mechanosensing and mechanoregulation of the extracellular matrix by aortic smooth muscle cells (5, 14, 15). Such deficits are believed to make the aortic wall vulnerable to dilation and dissection. An associated inability of adventitial fibroblasts to

Significance

Point mutations in the *ACTA2* gene encoding smooth muscle (SM) α-actin cause familial thoracic aortic aneurysms and dissections and predispose to premature coronary artery disease, stroke, and moyamoya disease. Studies on the mechanistic basis of these diseases are partly hampered by inability to collect affected tissues from living patients. Fibroblasts cultured from minimally invasive patient skin biopsies allowed study of *ACTA2*–R258C mutation-induced derangement in cell growth and interrogation of dysfunctional consequences of the mutation after induction of SM α-actin. Results show that R258C dominantly disrupts cytoskeletal properties attributed to SM α-actin and are consistent with deficiencies in multiple cytoskeletal functions. Information gathered from the patient-derived, cell-based assay strategies described herein has potential to facilitate understanding of disease progression mechanisms.

Author contributions: Z.L. and K.E.K. designed research; Z.L. and A.N.C. performed research; F.G., K.M.T., and D.M.M. contributed new reagents/analytic tools; Z.L., A.N.C., F.G., K.M.T., D.M.M., J.T.S., and K.E.K. analyzed data; and Z.L., A.N.C., and K.E.K. wrote the paper.

The authors declare no conflict of interest.

This article is a PNAS Direct Submission.

[1]To whom correspondence should be addressed. Email: kristine.kamm@utsouthwestern.edu.

This article contains supporting information online at www.pnas.org/lookup/suppl/doi:10.1073/pnas.1703506114/-/DCSupplemental.

sustain or restore a sufficiently strong adventitia may further lead to rupture (14).

We focus on the R258C mutation because of its prevalence in patients, its poor prognosis and high penetrance, and because it also causes moyamoya-like disease leading to cerebrovascular occlusion and stroke (6, 16). Lu et al. (17) investigated properties of expressed human R258C SM α-actin in vitro and found multiple defects, including impaired interaction with myosin, formation of less stable filaments, and enhanced levels of monomer. The R258 residue, which corresponds to amino acid R256 in the actin protein due to posttranslational processing that removes the N-terminal Met and Cys residues (18), lies at the interface between the two strands of filamentous actin. Mutation of R258 to C or H is understood to disrupt allosteric communication to binding sites on the surface of actin (17, 19). Intermediate effects on SM α-actin functions were observed in 1:1 mixtures of WT and R258C proteins, consistent with anticipated disruption of actin-dependent properties in heterozygous smooth muscle cells of patients harboring this mutation.

In the present study, we extend biochemical observations on R258C SM α-actin to fibroblasts isolated from patients that are heterozygous for *ACTA2*^{R258C}. Gaining insights on actin-based, disease-causing mutations in cells has been challenging, owing to the complex cellular environment with numerous actin-binding proteins, as well as the confounding presence of multiple actin isoforms (20). For aortic actinopathies, vascular muscle samples are rare, as aortas from affected individuals are seldom available and mouse models are currently lacking. We have implemented a human cell model to interrogate functional effects of mutant SM α-actin by inducing *ACTA2* expression from endogenous genes with myocardin-related transcription factor A (MRTF-A), a potent coactivator of smooth muscle contractile genes. This protocol effectively converts fibroblasts to myofibroblasts allowing a specific focus on SM α-actin–dependent properties (21). Our results are generally consistent with biochemical findings, namely expression of R258C SM α-actin inhibits, in an autosomal dominant manner, well-documented functional effects of WT SM α-actin on myofibroblast migration and contraction. Further, R258C SM α-actin appears to segregate predominantly to the soluble fraction of cellular actin where it may exert effects on cytoskeletal dynamics, as well as actin-dependent regulation of transcription.

Results

Immortalization of Dermal Fibroblasts from Normal Individuals and *ACTA2*$^{+/R258C}$ Patients. The catalytic subunit of human telomerase (h-TERT) was used to extend the lifespan of dermal fibroblasts to produce large, uniform quantities of cells for biochemical and cell biological assessments. Immortalized lines were compared with the uninfected primary cells of origin to verify extended lifespan by plotting population doubling versus time in culture (Fig. 1*A*). Primary (uninfected) cells from both controls and R258C patients entered senescence after 30–40 population doublings, which is in the normal range for adult donors (22, 23). Interestingly, R258C cells from both patients (P1 and P2) exhibited senescence later than those from controls (40 versus 30 population doublings, respectively). All immortalized cells, regardless of origin, exhibited an extended lifespan, growing well past the population doubling level at which senescence was induced in the corresponding primary samples (Fig. 1*A*). Additionally, all immortalized cells exhibited cellular morphology similar to primary cells in early passage (Fig. 1*B*).

We further characterized immortalized fibroblasts by comparing proliferation rates to those of primary cells (Fig. 2). Proliferation was assessed by fluorescence imaging of EdU-labeled DNA and quantifying EdU$^+$ cells (Fig. 2*A*). Proliferation rates of primary control cells decreased from 40 ± 2% at passage 10 to 22 ± 3% at passage 23 (Fig. 2*B*). Consistent with

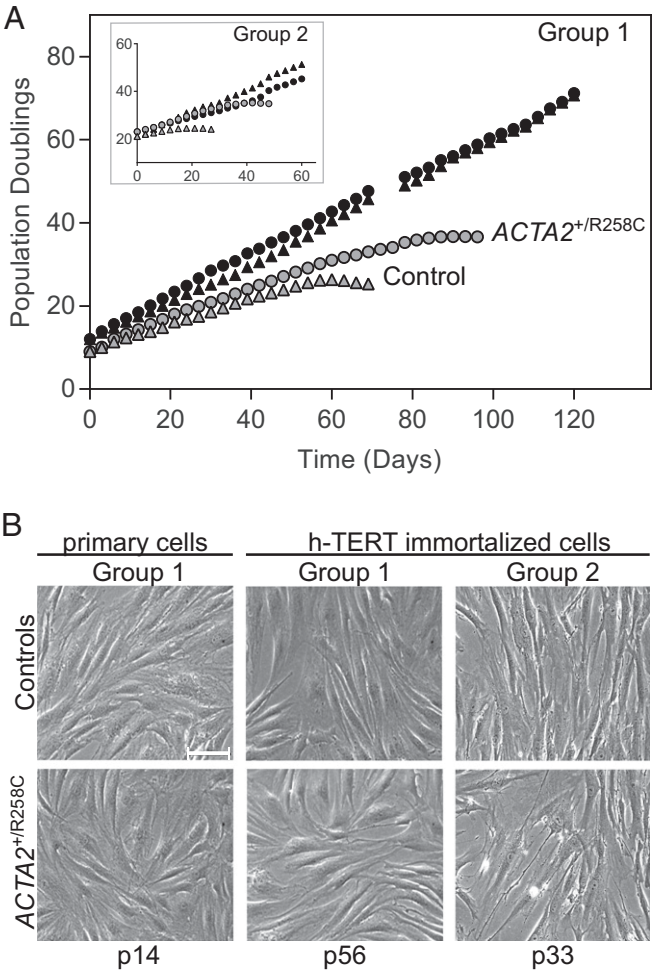

Fig. 1. Immortalization of human dermal fibroblasts characterized by cell growth curves and morphology. (*A*) In vitro life span of primary (gray symbols) and h-TERT–immortalized (black symbols) dermal fibroblasts from control volunteers (triangles) and patients with *ACTA2*–R258C mutation (circles). Results of cells from control C1 and patient P1 (group 1) are shown, with results from control C2 and patient P2 (group 2) in the *Inset*. Population doublings were conducted as described. (*B*) Phase contrast images of cells at indicated passage (p) number. Cell line identifications are as described in *A*. (Scale bar, 100 μm.)

the apparent delay in senescence observed for mutant cells, the proliferation rate for primary *ACTA2*$^{+/R258C}$ cells was not diminished between passages 10 and 23 (Fig. 2*B*). Proliferation rates for *ACTA2*$^{+/R258C}$ exceeded control (ratio ~1.7 at passage 23). Importantly, all h-TERT–infected cell lines maintained proliferation rates similar to cells in early passage, consistent with an immortalized phenotype (Fig. 2*B*).

The expression of SM α-actin in primary and immortalized fibroblasts was probed by immunofluorescence imaging (Fig. 2*A*). Primary cells showed gradual onset of SM α-actin expression with time in culture, however less so in R258C cells. Immortalized fibroblasts, similar to early passage primary cells, showed minimal staining for SM α-actin.

SM α-Actin Is Induced by MRTF-A in Control and *ACTA2*$^{+/R258C}$ Cells. To study effects of the *ACTA2*–R258C mutation on cytoskeletal functions in dermal fibroblasts, we induced SM α-actin expression by transfecting cells with replication-deficient adenovirus encoding MRTF-A (Ad-MRTF-A). MRTF-A is necessary and sufficient for myofibroblast differentiation in response to the

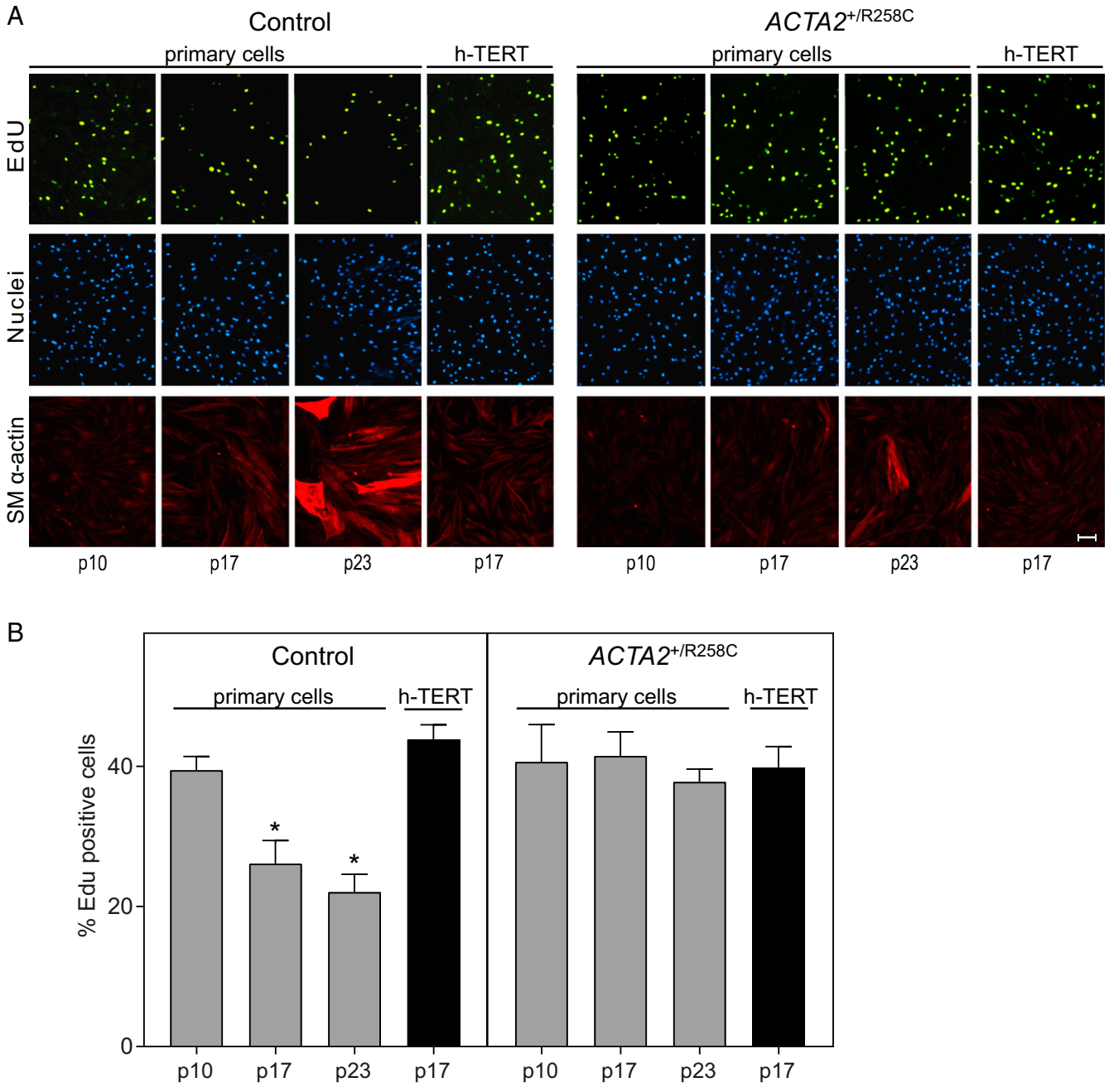

Fig. 2. Proliferation rates of primary and h-TERT–immortalized fibroblasts. (*A*) Control primary cells or *ACTA2*–R258C cells (group 1) at indicated passage (p) number or immortalized (h-TERT) were observed with epifluorescence microscopy to identify EdU^+ cells (green), Hoechst-stained nuclei (blue), and SM α-$actin^+$ cells (red). (Scale bars, 100 μm.) (*B*) Quantification of proliferation of group 1 cells estimated by $\%EdU^+$ cells. $^*P < 0.01$ compared with p10. Data are representative of at least three independent experiments and are expressed as the mean ± SEM.

established cytokine inducer, transforming growth factor β1 (TGF-β1) (21, 24, 25). Ad-MRTF-A was selected over TGF-β1 treatment owing to its shorter time (2 d versus 4–7 d) to achieve similar or greater (more than threefold versus more than twofold) increases in SM α-actin protein expression (21, 24–26). Both primary and immortalized, control and patient cells responded robustly and similarly to induction (Fig. 3*A*). Analysis of actin isoform distribution was performed by 2D gel electrophoresis and Western blotting with pan-actin antibody (Fig. 3*B*). Immortalized control cells increased SM α-actin expression from 7% to 36% of total actin in response to MRTF-A. The R-to-C mutation results in a shift in isoelectric point from 5.24 to 5.17 as shown with purified proteins, allowing quantitative measurement of mutant protein expression. Expression of both wild-type (WT) and mutant SM α-actin was confirmed in MRTF-A–treated cells from heterozygous patients, where total SM α-actin expression increased from 0% to ∼40% (with R258C–SM α-actin comprising 16–17% and WT 23–26% total actin) (Fig. 3*B*). Samples were further analyzed to determine fold changes in expression of vinculin and smooth muscle-specific proteins SM α-actin, SM22, and calponin in response to treatment (Fig. S1). MRTF-A induced significant increases in SM α-actin (approximately threefold) and calponin (approximately fourfold) that did not differ between control and $ACTA2^{+/R258C}$ mutant cells. No significant

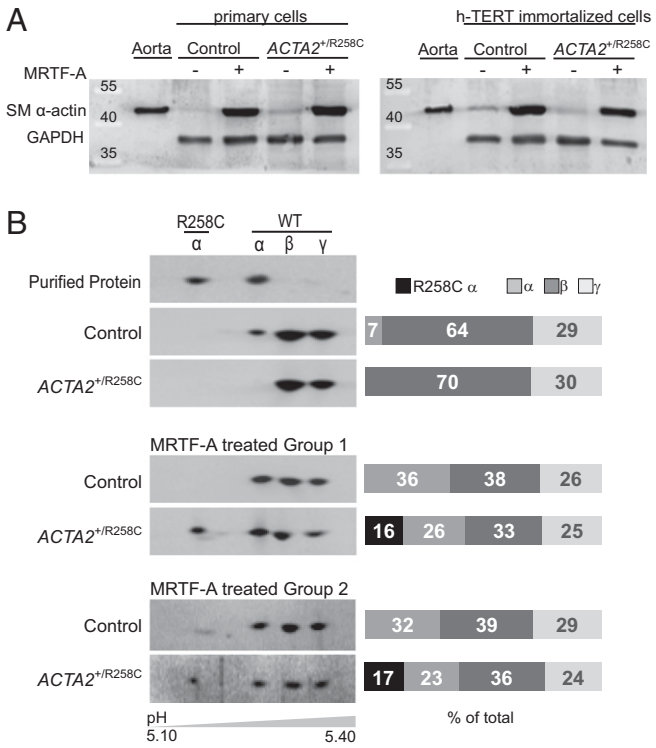

Fig. 3. Induction of SM α-actin by MRTF-A in primary and immortalized fibroblasts. (*A*) Representative immunoblots showing induction of SM α-actin 48 h after Ad-MRTF-A treatment in both primary and immortalized group 1 cells. Mouse aorta homogenate is control for SM α-actin. GAPDH is control for protein load. (*B*, *Left*) The 2D PAGE and immunoblotting with anti–pan-actin confirms induction of wild-type (WT) and mutant (R258C) SM α-actin in immortalized cells as indicated. Each panel is a blot from an SDS/PAGE gel for sample that had been separated in the first dimension by IEF with approximate pH range shown. Purified, expressed WT and R258C SM α-actins are standards for migration. The β- and γ-isoforms of actin are also present in cells. (*Right*) Quantification of isoform distribution in immunoblots at *Left*. Results are representative of at least three independent experiments.

changes were seen in vinculin or SM22 expression. The above results suggest that MRTF-A has similar effects on both control and mutant cells and support interpreting functional differences in relation to the mutant actin.

R258C Mutation in SM α-Actin Suppresses the Inhibitory Effects of WT SM α-Actin on Cell Migration. To examine the effects of *ACTA2*–R258C mutation on cytoskeletal functions, we compared control and R258C mutant fibroblasts with regard to cell migration, which has been shown to be inhibited by the expression of SM α-actin. Wound-healing assay measurements showed induction of SM α-actin by Ad-MRTF-A in control cells resulted in reduced number of cells migrating into the wound after 24 h by 18% compared with cells infected with Ad-GFP (Fig. 4 *A* and *B*). Expression of R258C SM α-actin eliminated the reduction in cell migration that was associated with increased WT SM α-actin (Fig. 4 *A* and *B*). To confirm the effects of WT and mutant SM α-actin on migration, we performed Transwell migration assays. The migration of control cells across a Transwell filter after 6 h was inhibited by 40% with induction of SM α-actin in controls, whereas there was no significant inhibition of migration on induction in R258C cells (Fig. 4 *C* and *D*). Thus, whereas R258C cells expressed similar amounts of total SM α-actin as controls, there was no reduction in cell motility by SM α-actin in mutant cells as assayed by wound healing and Transwell migration. Similar results were observed in migration assays performed on the second group of control and mutant cells (Fig. S2). Differences in cell migration upon induction of SM α-actin are well visualized in time-lapse video recordings of control (Movie S1) and R258C cells (Movie S2).

R258C Mutation in SM α-Actin Suppresses the Enhancing Effects of WT SM α-Actin on Matrix Contraction. To further examine the effects of R258C mutation on cytoskeletal functions, control and R258C cells were compared with regard to contractile properties as assayed by collagen matrix contractions (27). Two iterations of the collagen matrix model were assessed: floating matrix contraction (FMC) and stressed matrix contraction (SMC) (Fig. 5*A*). Control and R258C fibroblasts were embedded in collagen matrices and lattice contraction stimulated by the procontractile agonist FBS. Robust and similar induction of SM α-actin by MRTF-A was confirmed for all cell preparations (Fig. 5*B*). For FMC, matrices containing equal numbers of cells were released from culture surfaces soon after matrix polymerization and fixed for morphometry after 4 h in BSA or FBS (Fig. 5*C*). In this protocol, cells remodel the matrix under low tension conditions by protrusion and retraction of actin-containing dendritic extensions. FMC was quantified as the difference in area between gels treated with BSA or FBS. Induction of SM α-actin in control cells resulted in a significant increase in contraction as quantified by reduction in matrix area (Fig. 5*C*). However, induction of SM α-actin in R258C cells abrogated the expected change in floating matrix contraction.

For SMC, matrices containing equal numbers of cells remain attached to the culture surface for 18 h in BSA or FBS, following which they are released and fixed after 1 h (Fig. 5*A*). In this protocol, cells remodel the matrix leading to a high cell-matrix tension state where cells and collagen become aligned parallel to the culture surface, and prominent actin stress fibers and focal adhesions (FAs) form (27). Release of the matrix leads to a contraction that reflects dissipation of stress that was actively developed by cells in the matrix. SMC was quantified as the difference in area between gels treated with BSA or FBS. Like FMC, induction of SM α-actin in control cells resulted in a significant increase in SMC as quantified by reduction in matrix area upon release from the culture surface (Fig. 5*D*). Further, induction of SM α-actin in R258C cells led to no significant change in stressed matrix contraction.

R258C Mutation in SM α-Actin Diminishes Stress Fiber and FA Formation Brought About by WT SM α-Actin. To assess the effects of R258C mutation on gross cytoskeletal structure, control and mutant fibroblasts were cultured on glass coverslips with or without MRTF-A treatment. Fixed cells were stained for SM α-actin or vinculin and for F-actin (phalloidin). Both control and mutant cells without MRTF-A treatment appeared elongated and showed negligible staining for SM α-actin. F-actin staining by phalloidin revealed thin stress fibers seen primarily in the cell periphery (Fig. 6). Additionally, untreated cells exhibited small vinculin-containing FAs. Induction by MRTF-A in control cells led to robust staining for SM α-actin primarily colocalized with F-actin. Cells acquired a polygonal shape with abundant, thick α-actin–containing stress fibers. MRTF-A induction in control cells also led to an apparent increase in number of vinculin-containing FAs visualized at the ends of abundant linear stress fibers (Fig. 6).

Induction by MRTF-A in R258C cells resulted in SM α-actin staining that was both colocalized with F-actin and diffuse in the same cell (Fig. 6). Induction led to an apparent increase in number of stress fibers, but not to the extent observed with control cells (Fig. 6, enlarged panels, *Left* set). Similar to control fibroblasts, SM α-actin induction in R258C cells led to an increase in number of vinculin-containing FAs; however, the response appeared less than observed in control cells (Fig. 6, enlarged panels, *Right* set). Quantification of cell areas and number of FAs revealed that

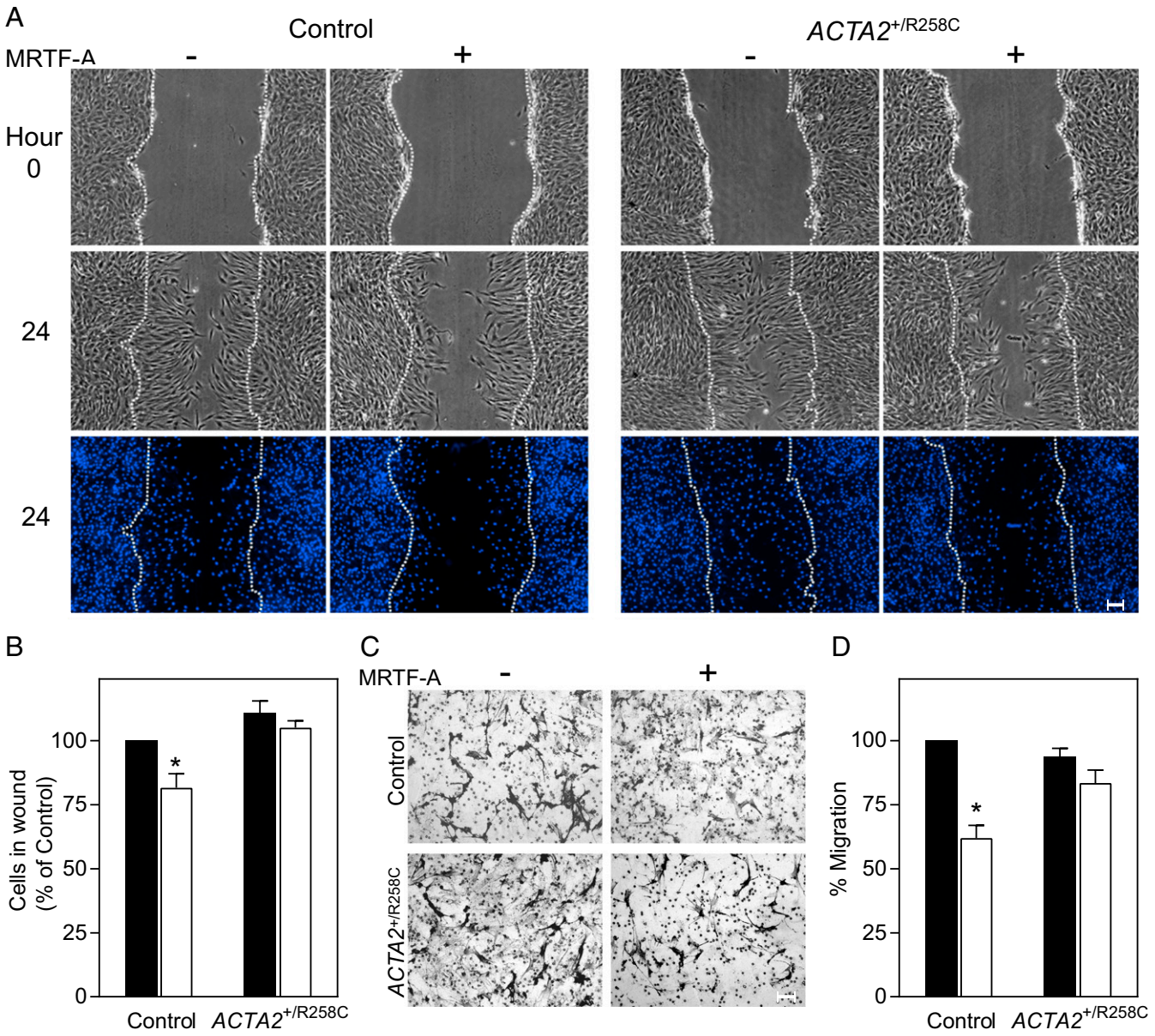

Fig. 4. R258C SM α-actin does not retard cell migration, unlike WT SM α-actin. (*A*) Representative phase contrast images for group 1 control and *ACTA2*$^{+/R258C}$ cells pretreated for 48 h with/without Ad-MRTF-A. Phase contrast images are from start of assay (0 h) and after 24 h. Epifluorescence images of nuclei stained with Hoechst at 24 h. Location of initial scratch margins indicated by dashed white lines. (Scale bars, 100 μm.) (*B*) Quantified effects of SM α-actin variant on migration. Closed bars, MRTF-A $^{-}$; open bars, MRTF-A $^{+}$. Data analysis was performed as described with control MRTF-A^{-} as 100%. $n = 3$ for three independent cell preparations. *$P < 0.01$. (*C*) Representative images of Transwell membranes with cells stained by crystal violet. Membranes were fixed 6 h after seeding. Cells were prepared as in *A*. (Scale bars, 100 μm.) (*D*) Quantified effects of SM α-actin variant on migration. Closed bars, MRTF-A $^{-}$; open bars, MRTF-A $^{+}$. Data analysis was performed as described with control MRTF-A^{-} as 100%. $n = 3$ for three independent cell preparations. *$P < 0.01$ compared with control MRTF-A^{-}.

MRTF-A–treated mutant cells compared with controls were about 40% smaller (6,235 ± 371 versus 10,463 ± 803 μm^2) and contained roughly half the number of FAs per cell (580 ± 71 versus 1,117 ± 95). The difference in FA number resulted from fewer FAs <2 μm^2 (Fig. S3). These results align with the hypothesis that R258C SM α-actin may be preferentially distributed in a nonfilamentous pool of actin, thus limiting the ability of SM α-actin to effect stress fiber and FA formation.

R258C Mutation in SM α-Actin Increases the Pool of Soluble SM α-Actin in Comparison with That in Control Cells. To test the hypothesis that R258C SM α-actin is disproportionately distributed in the soluble actin fraction, control and mutant cells were collected and fractionated to define proportions of F- and G-actin. Pellet (F-actin) and supernatant (G-actin) fractions were separated by centrifugation and analyzed by SDS/PAGE and Western blot. Induction of SM α-actin in control cells led to an SM α-actin F-/G-actin ratio of 0.81 ± 0.09, whereas induction of SM α-actin in R258C patient cells led to a ratio of 0.45 ± 0.11 (Fig. 7 *A* and *B*), consistent with a preferential distribution of SM α-actin in the soluble, G-actin fraction in R258C cells. To determine whether R258C SM α-actin incorporates into F-actin, cell fractions were further analyzed by 2D PAGE. Fig. 7*C* shows that the SM α-actin distribution in control cells is similar to that observed in 1D PAGE, whereas WT SM α-actin appears enriched in the F-fraction of R258C cells. R258C SM α-actin may incorporate into F-actin, but

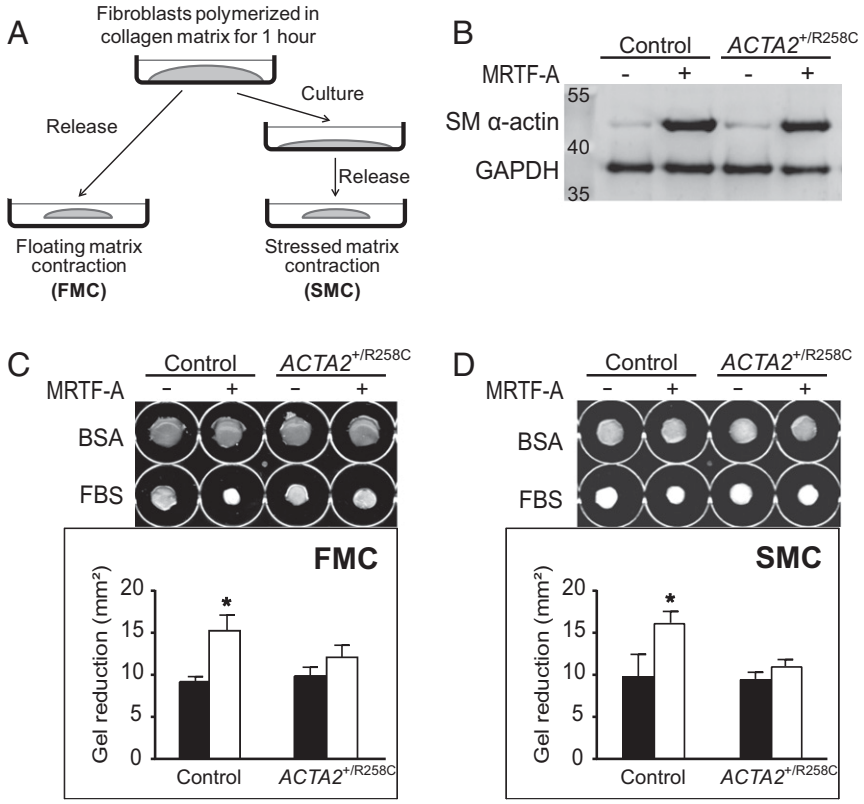

Fig. 5. R258C SM α-actin inhibits the enhancement of matrix contraction by WT SM α-actin. (*A*) Schematic illustrating two models of matrix contraction. Floating matrix contraction (FMC) occurs when cell-containing matrices are released from culture surfaces soon after matrix polymerization. Stressed matrix contraction (SMC) occurs when cell-containing matrices remain attached to the culture surface so that cells develop isometric tension in the matrix. The matrix is released after 18 h, resulting in a contraction. *A* is adapted with permission from ref. 58. (*B*) Representative immunoblot for induction of SM α-actin in group 1 cells used in matrix contraction assays. Cells were collected 48 h after ±Ad-MRTF-A. (*C*, *Upper*) Representative images of collagen gels at endpoint of FMC assay. (*Lower*) Quantified effects of SM α-actin variant on FMC. Closed bars, MRTF-A $^{-}$; open bars, MRTF-A $^{+}$. (*D*, *Upper*) Representative images of collagen gels at endpoint of SMC assay. (*Lower*) Quantified effects of SM α-actin variant on SMC. Closed bars, MRTF-A $^{-}$; open bars, MRTF-A $^{+}$. Gel areas were analyzed with ImageJ and contraction was calculated as: gel area reduction = (area in BSA) − (area in FBS). $n = 3$, for three independent cell preparations for each assay. *$P <$ 0.05 compared with control MRTF-A^{-}.

to a significantly lower extent than WT SM α-actin. Importantly, R258C SM α-actin is enriched in the G-actin, soluble fraction of R258C cells.

Discussion

The R258C mutation in SM α-actin suppresses, in a dominant negative manner, myofibroblast migration and contraction behaviors attributed to induction of WT SM α-actin. The effects are likely due, at least in part, to a reduction in SM α-actin–containing filaments that play a key role in effecting these behaviors. Our findings are significant in establishing cytoskeletal effects of the mutation in a cellular context with the *ACTA2*$^{+/R258C}$ genotype. Thoracic aortic aneurysms and dissections are understood to result from dysfunctional mechanosensing and mechanoregulation of the extracellular matrix by intramural cells, leading to compromised structural integrity of the aortic wall (14). Our results point to the possibility that, in addition to affecting vascular smooth muscle cells, *ACTA2* mutations may also compromise adventitial myofibroblasts in responding to mechanical stresses and remodeling the adventitial sheath to protect against rupture.

The patient dermal fibroblast model offers advantages for interrogating effects of genetic mutations in SM α-actin. These fibroblasts are relatively easily obtained from patients and isolated for cell culture. They are readily immortalized by the human telomerase catalytic subunit, h-TERT, preventing the erosion of telomeres, and circumventing the induction of senescence (28, 29). Our results show that expression of h-TERT efficiently extended the lifespan of subject fibroblasts and yielded a uniform population of cells for experimental purposes. Interestingly, we noted that primary R258C cells from patients exhibited delayed senescence and maintained proliferative capacity beyond primary cells from controls. Reduction in proliferation was associated with increased expression of SM α-actin. Whereas these observations were incidental to the characterization of immortalized cells, they are consistent with results showing greater proliferation by primary smooth muscle cells and fibroblasts from patients heterozygous for other *ACTA2* mutations, as well as from *Acta2*$^{-/-}$ mice (16, 30). In vivo, vascular smooth muscle hyperplasia in response to carotid artery injury greatly exceeded wild-type in *Acta2*$^{-/-}$ mice (30). These and other results implicate SM α-actin in the inhibition of proliferation (31). The present observations align with the hypothesis that R258C SM α-actin disrupts an inhibitory effect of wild-type SM α-actin on proliferation, permitting hyperplastic vascular occlusions, leading to stroke (16). Further studies will be required to elucidate cellular mechanisms, as well as environmental queues by which particular *ACTA2* mutations result variously in stroke or coronary artery disease, in addition to TAAD.

The role of SM α-actin in fibroblasts has received significant attention, as its expression is a hallmark for the modulation of fibroblast to myofibroblast phenotype (12, 32, 33). A powerful regulator of this modulation is TGF-β1, which induces SM α-actin protein and mRNA expression in both growing and quiescent fibroblasts (26). TGF-β1 induction of the myofibroblast

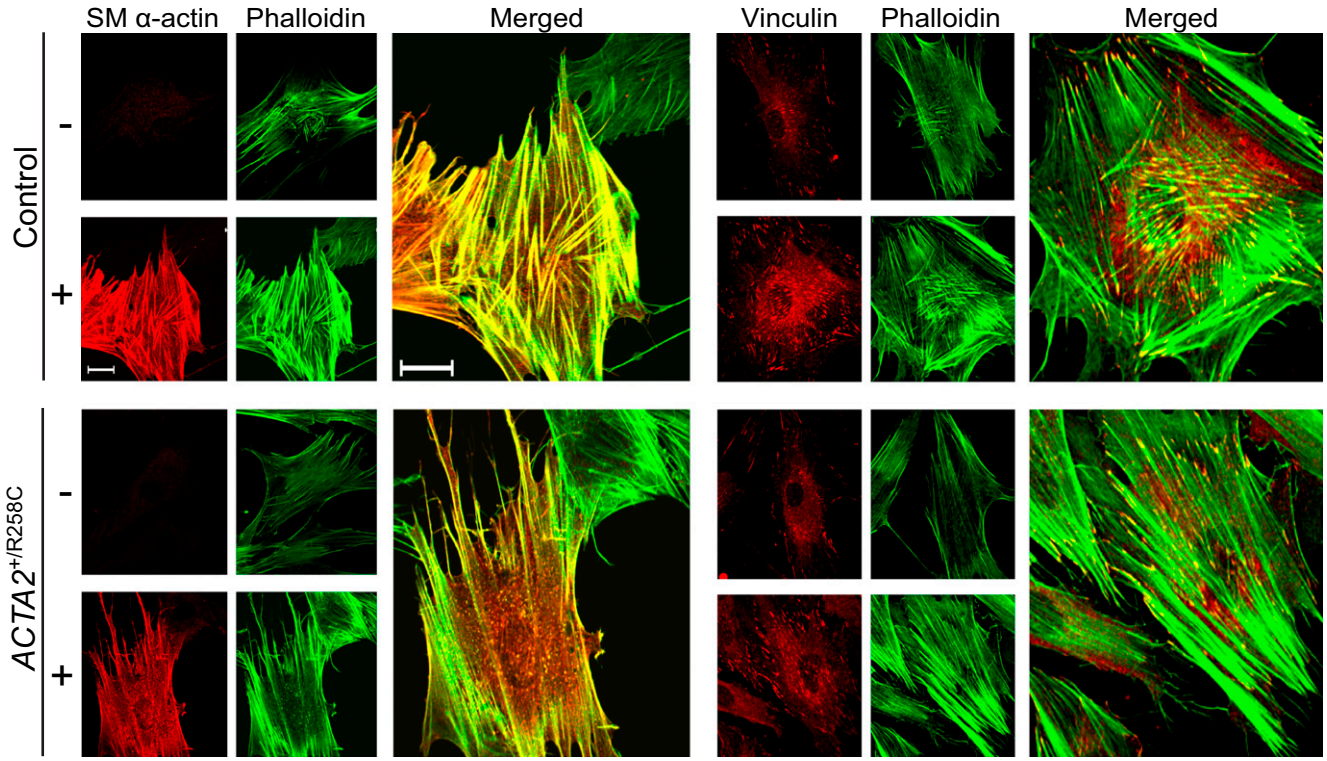

Fig. 6. Induction of SM α-actin in R258C cells results in less prominent stress fibers and focal adhesions than in control cells. Representative confocal micrographs of control (*Upper*) and R258C (*Lower*) cells infected with (+) or without (–) Ad-MRTF-A for 48 h followed by subculture overnight with fixation and staining as described. (*Left* set) SM α-actin immunofluorescence (red) and Alexa-488 phalloidin-stained F-actin (green). Enlarged image represents merge of MRTF-A$^-$–induced cells. (*Right* set) Representative confocal micrographs of vinculin immunofluorescence (red) and Alexa-488 phalloidin-stained F-actin (green). Enlarged image represents merge of MRTF-A–induced cells. (Scale bars, 20 μm.)

phenotype is dependent upon the serum response factor (SRF) transcriptional coactivator MRTF-A, as MRTF-A null or deficient fibroblasts fail to induce SM α-actin in response to TGF-β1 (21, 24, 25). MRTF-A is sequestered in the cytoplasm by interactions with G-actin (34). Stress signals that promote F-actin polymerization lead to nuclear accumulation of MRTF-A where the MRTF-A/SRF complex binds to consensus elements within promoters of smooth muscle-specific target genes, primary of which is *ACTA2* (34). In the present study we have bypassed extracellular signaling to induce *ACTA2* by expression of MRTF-A, which was previously shown to be effective in promoting the myofibroblast phenotype (21, 25). We found changes in protein expression that were consistent with those made by others (24, 25). MRTF-A treatment resulted in rapid and robust expression of SM α-actin that was comparable in control and mutant cells. Additionally, no differences between control and mutant cell responses were found for vinculin, SM22, or calponin. These findings support interpretations that ascribe functional differences to the actin mutation.

The myofibroblast model affords the opportunity to examine effects of R258C SM α-actin in a complex intracellular environment. Effects of the mutation on fibroblast motility and contraction are remarkably consistent with predictions from biophysical studies on expressed vascular actins, but not unsurprisingly so. In vitro studies with expressed actins showed that the R258C mutation leads to defects in multiple facets of SM α-actin properties, including reduced actin filament stability and less productive interactions with smooth muscle myosin (17). However, in 50:50 mixtures of WT and R258C, polymerization rates were intermediate and skewed more toward the rate observed for WT SM α-actin. R258C filaments were propelled at slower speeds by smooth muscle myosin in in vitro motility assays, and the effect scaled with the fraction of mutant actin in the filaments. In MRTF-A–treated fibroblasts, induction of SM α-actin leads to a shift in isoform distribution from 70:30 β:γ to 40:35:25 α:β:γ. In mutant cells, R258C comprises less than 20% of total actin. Thus, its impact on actin-dependent functions in this cell model might have been imperceptible. However, by focusing on behaviors brought about by the induction of SM α-actin, effects of the mutation were readily detected. In two models each of cell migration and matrix contraction, R258C SM α-actin reversed the effect of WT SM α-actin such that these behaviors were not different from those in uninduced fibroblasts. Thus, we speculate that R258C SM α-actin may preferentially disrupt SM α-actin–containing filaments, compared with β- and/or γ-actin–containing filaments.

Myofibroblasts exhibit cytoskeletal features, including SM α-actin–rich stress fibers attached to FAs, which enable them to remodel and contract the extracellular matrix and also to adapt their activity to changes in the mechanical microenvironment. Fibroblast cell shape features correlate with SM α-actin presence where α-actin$^+$ cells have larger average areas and more and larger FAs than α-actin$^-$ cells (35). Herein, MRTF-A–induced control fibroblasts spread to ~10^4 μm^2, comparable to reported values (35), whereas R258C fibroblasts were significantly smaller despite similar expression of SM α-actin. Mutant fibroblasts were not only smaller, but had fewer FAs. These observations are consistent with findings by others, where FA number correlates with cell size, and it is thought that global shape of cells plays an important role in control of FA assembly and organization through mechanical tension in the cytoskeleton (36, 37). SM α-actin promotes high actin–myosin contractile activity leading to formation of thick stress fibers that are implicated in the time-dependent maturation of vinculin-containing FAs in myofibroblasts (38–41). FA categories and size ranges have been described for human Dupuytren's fibroblasts as immature

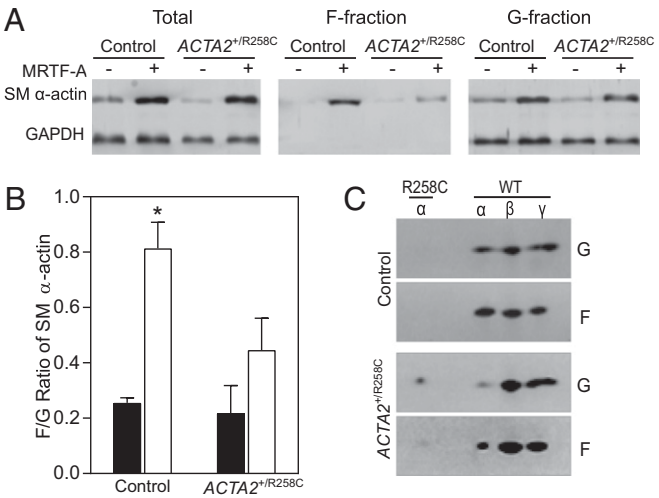

Fig. 7. Induction of SM α-actin in R258C cells results in decreased F/G actin ratio in comparison with that in control cells. (*A*) Representative immunoblots showing distribution of SM α-actin in pellet and supernatant fractions. Samples were prepared as described. Pellets (F) were resuspended in volume equal to supernatant (G) and equal volumes loaded for SDS/PAGE and immunoblotting. (*B*) Quantified effects of SM α-actin variant on F/G SM α-actin ratio. Closed bars, MRTF-A$^-$; open bars, MRTF-A$^+$. $n = 3$, for three independent cell preparations. *$P < 0.01$. (*C*) Representative 2D PAGE and immunoblotting for SM α-actin in F and G fractions from control and R258C cells. $n = 3$.

(<2 μm^2), mature (2–6 μm^2), and supermature (>6 μm^2), the latter categories associated with the presence of SM α-actin (41). Surprisingly, we found no difference in number of mature FAs between control and mutant cells, which may owe in part to the shorter duration of induction by MRTF-A versus TGF-β1 (2 versus 5 d). The dynamics of FA assembly and turnover in these cells will require further study. Whereas induction of SM α-actin by MRTF-A led to increased stress fibers and focal adhesions in both control and R258C cells, the prominence of both stress fibers and FAs was less in images of mutant cells. Similar observations were made in cultured smooth muscle cells from patients with other *ACTA2* mutations (7). This effect may result from lower α-actin filament stability, greater susceptibility to cleavage by cofilin and/or impaired actomyosin force generation, all of which were observed with expressed proteins in vitro (17). Consistent with the disrupting effects of R258C SM α-actin on filament stability, the ratio of F/G SM α-actin was significantly reduced in mutant cells, again confirming the impact of this mutation in a cellular context.

The highly dynamic actin cytoskeleton plays a key role in cell migration through controlled assembly and disassembly of actin filaments as well as FAs. It is likely that SM α-actin stabilization of stress fibers and FAs retards cell migration. By varying SM α-actin content through different approaches, several laboratories have correlated increased α-actin with inhibition of fibroblast migration (31, 42, 43). We confirmed such an effect on induction of SM α-actin in control cells in both the scratch and Transwell migration assays. However, in patient fibroblasts with the R258C mutation, the retarding effect is absent, thus demonstrating a dominant functional defect brought about by the mutant actin.

Fibroblasts cultured in 3D collagen matrices contract the lattice in an actin-dependent manner (44–46), and the extent of matrix contraction has been correlated with cellular contents of SM α-actin (40, 47). The present results show that induction of SM α-actin in control fibroblasts has a significant potentiating effect on both low- and high-tension matrix contractions. Further, expression of R258C SM α-actin abolishes enhancement of contraction, consistent with the hypothesis that the mutation impacts SM α-actin–dependent processes in cells.

How the functional phenotypes in myofibroblasts translate to aortic smooth muscle needs to be considered in light of the roles of actin in vascular smooth muscle where it is critical for force production and maintenance of the submembrane cytoskeleton that strengthens connections between contractile proteins and the extracellular matrix (13). Additionally, actin plays an important role in modulating transcription of vascular muscle contractile protein genes via its interaction with MRTF-A. Extrapolating from the deleterious impact of R258C SM α-actin on myosin-dependent force production with isolated thin filaments (17) and on mutant fibroblast matrix contractions (herein), we hypothesize that aortic smooth muscle force production will be compromised in patients with the R258C *ACTA2* missense mutation, leading to dysfunctional mechanical homeostasis and structural failure (14). Interestingly, affected individuals show little disruption in function of nonvascular smooth muscle tissues (16). This finding may be related to the higher content of SM α-actin versus SM γ-actin in vascular tissues (9) and/or to the limited regulatory reserve in aortic smooth muscle (48). More severe than R258, mutation of *ACTA2* R179 has the greatest risk of an aortic event and is unique in causing multisystemic smooth muscle dysfunction extending to visceral organs that have a higher proportion of SM γ-actin (6, 49). Of note, mutation of this residue leads to very severe defects in polymerization that likely exert negative effects, although present in small proportion (50). Studies on fibroblasts from *ACTA2* R179C patients will likely reveal more profound deficits than seen with R258C.

In addition to interfering with F-actin–dependent force production, R258C SM α-actin was enriched in the soluble G-actin fraction of myofibroblasts where it may exert effects on cytoskeletal dynamics, as well as actin-dependent transcriptional regulation. Cellular actin dynamics are complex, where polymerization of G-actin into F-actin is reversible and both reactions are regulated by numerous actin binding proteins. Lu et al. (17) predicted that the pool of monomeric actin would increase relative to wild-type cells because R258C SM α-actin has a higher critical concentration, a higher affinity for profilin, and is more susceptible to severing and shortening by cofilin. The present results confirm this prediction; however, the specific reactions involved remain to be investigated.

In aggregate, biochemical and cellular assays are consistent with an autosomal dominant effect of the R258C mutation on various SM α-actin–dependent properties and processes, including force production and actin assembly. In the setting of a majority fraction of SM α-actin in aortic smooth muscle, these effects are likely to be amplified. The natural history of TAAD in the setting of *ACTA2* missense mutations may develop through defects in multiple functions of SM α-actin. Animal models of these diseases are needed to shed light on involved processes.

Experimental Procedures

Human Fibroblast Culture and Immortalization. Skin biopsies from patients heterozygous for *ACTA2*–R258C (*ACTA2*$^{+/R258C}$) and unaffected controls (WT) were obtained with informed consent and approval by the University of Texas (UT) Health Science Center at Houston Institutional Review Board. The sample groups were as follows: group 1, a 7-y-old affected male and a 26-y-old control male; and group 2, a 27-y-old affected female and a 25-y-old control male. *ACTA2* genotypes were confirmed by DNA sequencing. Skin biopsies were explanted in culture to obtain dermal fibroblasts. Deidentified primary fibroblast lines were sent to the University of Texas Southwestern Medical Center for studies described herein as approved by the UT Southwestern Institutional Review Board. Cells were cultured in DMEM plus10% FBS and 100 units/mL penicillin and 100 μg/mL streptomycin (HyClone, Thermo Scientific) in a 37 °C and 5% CO_2 humidified incubator. Immortalization of fibroblasts was carried out by infection with retroviral supernatants obtained from packaging cells stably expressing h-TERT cloned into the pBabePuro vector (51). After 48-h infection, cells were selected for 2 wk with puromycin at 1 μg/mL. Immortalization was confirmed by telomerase activity and length analysis as previously published (52, 53).

Population Doubling and Proliferation of Primary and Immortalized Cells. Population doubling numbers were determined for primary and immortalized, control and patient cells. Cells were seeded on six-well plates (1×10^5 per well), then collected by centrifugation after trypsin treatment at 3 d. Cell pellets were resuspended and counted. The 1×10^5 cells were reseeded on a six-well plate and cultured 3 d for subsequent counting. Population doubling curves were generated as population doubling versus days in culture. Cell population doubling number was calculated according to the formula: $n = 3.32$ (log Xe − log Xb) + S, where Xb is the cell number at the beginning of the incubation (1×10^5), Xe is the cell number at the end of the incubation, and S is the doubling level used to initiate the subculture. Cell proliferation rates were measured with the Click-iT EdU Imaging Kit (Invitrogen), following the recommended protocol with minor modification. Briefly, cells were seeded on coverslips overnight, followed by culture in 10 μM EdU for 20 h. EdU-treated cells were fixed in 3.7% paraformaldehyde in PBS for 15 min at room temperature, then permeabilized for 20 min in 0.5% Triton X-100 in PBS. EdU incorporation was detected following kit instructions, and fixed cells were subsequently stained for nuclei (Hoechst) and SM α-actin (A2547, Sigma). Five microscopic images of each sample were collected for analysis. Cell proliferation rates were calculated as numbers of EdU^+ cells per numbers of nuclei (% EdU^+ cells).

Immunoblot and Isoelectric Focusing. Samples were loaded by total protein (concentrations determined by Bradford protein assay) or by calculated cell number. For immunoblots, samples were boiled in Laemmli buffer, subjected to SDS/PAGE, transferred onto nitrocellulose membrane, immunoblotted using routine procedures, then detected by chemiluminescence with the Pierce ECL Western blotting substrate (Thermo Scientific). Images were acquired using a Storm Imaging System (GE Healthcare). Primary antibodies against the following proteins were used for immunoblotting: SM α-actin (A2547, Sigma), vinculin (V9131, Sigma), calponin (C2687, Sigma), SM22 (Abcam), and GAPDH (Santa Cruz). Secondary antibodies were goat anti-mouse or rabbit HRP (Jackson ImmunoResearch). For separation of R258C mutant SM α-actin from WT actin by isoelectric focusing (IEF), pelleted cells or purified proteins were lysed and solubilized directly in ReadyPrep 2D Starter Kit Rehydration/Sample Buffer (Bio-Rad), then subjected to fractionation in a 24-cm, pH 4–7, immobilized pH gradient gel strip (GE Healthcare). Samples were focused for a total of 100 kilovolt hours in a PROTEAN IEF Cell (Bio-Rad). The maximum voltage was 10 kV and current was limited to 50 μA per strip. After IEF, the portion of gel strip that corresponded to pH 5.1–5.4 was subjected to 10% SDS/PAGE, then immunoblotted using routine procedures.

"Wound"-Induced Cell Migration and Time-Lapse Microscopy. Immortalized human dermal fibroblasts grown to ∼60% confluence were infected with Ad-MRTF-A or Ad-GFP at 80 multiplicity of infection (MOI) in DMEM containing 10% FBS for 24 h (21, 24). Following an additional 24 h in DMEM containing 10% FBS, cells were collected and replated onto six-well plates. Viral titrations with Ad-GFP showed >90% of cells expressed GFP at 80 MOI with no effect on cell growth or morphology. Cell confluent monolayers were washed and scratch wounds were applied with a 1-mL pipette tip. Live-cell images were collected by an inverted phase contrast microscope (Eclipse Ti, Nikon) immediately after wound creation (0 h). Plates were returned to incubator and cells allowed to grow and migrate for 24 h. Hoechst 33342 was added to stain nuclei, followed by collection of phase contrast and nuclear staining images. The number of cells that migrated into the wound region was quantified by counting the number of nuclei. Time-lapse cell migration videos were assembled with images acquired by the Eclipse Ti equipped with an on-stage chamber providing routine incubation conditions (37 °C, 5% CO_2). Images, collected at 15-min intervals for 24 h, were acquired and processed with a CoolSNAP ES2 camera (Photometrics) and NIS Elements imaging software (54).

Transwell Migration. Cells were infected with Ad-MRTF-A or Ad-GFP for 48 h, released by trypsin, centrifuged, and counted. An equal number of cells (5×10^4) in serum-free medium were seeded on 8.0-μm pore collagen-coated cell culture inserts (353097, BD Falcon) with medium containing 10% FBS (600 μL) in the lower compartment of the 24-well plate. After 6-h incubation, medium was aspirated from both insert and lower well. Cells inside the insert were gently removed using cotton swabs. Inserts, with migrated cells attached to the underside, were then fixed with 3% formaldehyde in PBS and visualized by light microscopy. Images were acquired from five random fields and the numbers of stained cells counted.

Floating and Stressed Collagen Matrix Contraction. Methods for preparing cell-containing collagen matrices have been described previously (55). Briefly, cell-containing collagen matrices (200 μL, 1.5 mg/mL bovine type I collagen, 2×10^5 cells per matrix) were polymerized, plating on the bottom of 24-well plates in a humidified incubator at 37 °C. For floating matrix contraction, polymerized matrices were released from the culture surface after 1 h and incubated for 4 h in DMEM containing 5 mg/mL BSA or 10% FBS. For stressed matrix contraction, polymerized matrices were cultured overnight in DMEM with BSA or FBS, rinsed with DMEM, and then released from the culture surface and incubated for 1 h. At the end of either procedure, samples were fixed with 3% paraformaldehyde in PBS. Images of collagen matrices were obtained with an Epson photo scanner. Gel area was analyzed using ImageJ and contraction calculated as: gel area reduction = (area in BSA) − (area in FBS).

Immunofluorescence and Confocal Microscopy. Cells were seeded onto glass coverslips overnight, fixed with 3% paraformaldehyde/PBS, blocked with 3% BSA/PBS, and permeabilized with 0.5% Triton X-100/PBS. The coverslips were then incubated with primary antibodies for 2 h at room temperature or overnight at 4 °C, then washed three times in PBS before incubation with second antibody for 1 h. F-actin was stained with 1:1,000 dilution of Alexa-Fluor 488 phalloidin. Protein-specific primary antibodies were imaged using Alexa-Fluor 568-conjugated secondary antibodies against mouse or rabbit IgG (Invitrogen-Molecular Probes). Coverslips were mounted onto glass slides with Fluoromount-G, and images were collected with an epifluorescence (Eclipse E400, Nikon) or confocal microscope (LSM510, Zeiss). Acquired images were processed with LSM Image Browser software. Cell areas were estimated by the cut-and-weigh method using images of cells stained by Alexa-Fluor 488 phalloidin. Focal adhesions were analyzed using the Focal Adhesion Analysis Server to quantify images of cells stained by immunofluorescence for vinculin (56, 57).

Actin Fractionation. Confluent monolayers of cells were subjected to serum withdrawal for 6 h, leading to depolymerization of actin, as confirmed by negligible staining by phalloidin. Cells were then cultured in medium containing 10% FBS for 16–18 h to allow repolymerization of cellular actin. Distribution of actin in soluble (G) and filamentous (F) fractions was measured by the G-actin/F-actin In Vivo Assay Kit as described by the manufacturer for adherent cells (BK037, Cytoskeleton). Briefly, cells were lysed in F-actin stabilization buffer (Pipes 50 mM, pH 6.9, NaCl 50 mM, $MgCl_2$ 5 mM, EGTA 5 mM, ATP 1 mM, glycerol 5%, Nonidet P-40 0.1%, Triton X-100 0.1%, Tween 20 0.1%, 2-mercapto-ethanol 0.1%, and protease inhibitor mixture) at 37 °C for 30 min. Large lysate debris was precleared by gentle centrifugation at 350 × *g* for 5 min at room temperature, and the resulting supernatant was then subjected to centrifugation at 100,000 × *g* at 37 °C for 1 h. The supernatant (S) was collected and the F-actin–containing pellet resolublized in 100 μL of F-actin depolymerization buffer on ice for 1 h, pipetting up and down several times every 15 min to help pellet resuspension. Equivalent volumes of input, supernatant, and pellet fractions were analyzed by SDS/PAGE, IEF, and immunoblot.

Statistical Analysis. All data shown represent at least three independent experiments. Data are expressed as mean ± SEM. Statistical analysis was carried out using GraphPad Prism software.

ACKNOWLEDGMENTS. We thank Jerry Shay, Woodring Wright, Brody Holohan, and Ryan LaRanger for reagents and advice concerning cell immortalization, and Robert Gerard and Eric Olson for reagents and advice concerning MRTF-A adenovirus. This work was supported by NIH Grants P01 HL110869 and R01 HL109942.

1. National Center for Injury Prevention and Control (2007) WISQARS Leading Causes of Death Reports, 1999–2007. Available at https://webappa.cdc.gov/sasweb/ncipc/leadcaus10.html. Accessed December 6, 2016.
2. Elefteriades JA, Farkas EA (2010) Thoracic aortic aneurysm clinically pertinent controversies and uncertainties. *J Am Coll Cardiol* 55:841–857.
3. Goldfinger JZ, et al. (2014) Thoracic aortic aneurysm and dissection. *J Am Coll Cardiol* 64:1725–1739.
4. Milewicz DM, et al. (2008) Genetic basis of thoracic aortic aneurysms and dissections: Focus on smooth muscle cell contractile dysfunction. *Annu Rev Genomics Hum Genet* 9:283–302.
5. Karimi A, Milewicz DM (2016) Structure of the elastin-contractile units in the thoracic aorta and how genes that cause thoracic aortic aneurysms and dissections disrupt this structure. *Can J Cardiol* 32:26–34.
6. Regalado ES, et al.; Montalcino Aortic Consortium (2015) Aortic disease presentation and outcome associated with ACTA2 mutations. *Circ Cardiovasc Genet* 8:457–464.
7. Guo DC, et al. (2007) Mutations in smooth muscle alpha-actin (ACTA2) lead to thoracic aortic aneurysms and dissections. *Nat Genet* 39:1488–1493.
8. Milewicz DM, et al. (2010) Genetic variants promoting smooth muscle cell proliferation can result in diffuse and diverse vascular diseases: Evidence for a hyperplastic vasculomyopathy. *Genet Med* 12:196–203.

9. Fatigati V, Murphy RA (1984) Actin and tropomyosin variants in smooth muscles. Dependence on tissue type. *J Biol Chem* 259:14383–14388.
10. Glukhova MA, et al. (1988) Modulation of human aorta smooth muscle cell phenotype: A study of muscle-specific variants of vinculin, caldesmon, and actin expression. *Proc Natl Acad Sci USA* 85:9542–9546.
11. Gabbiani G, et al. (1981) Vascular smooth muscle cells differ from other smooth muscle cells: Predominance of vimentin filaments and a specific alpha-type actin. *Proc Natl Acad Sci USA* 78:298–302.
12. Tomasek JJ, Gabbiani G, Hinz B, Chaponnier C, Brown RA (2002) Myofibroblasts and mechano-regulation of connective tissue remodelling. *Nat Rev Mol Cell Biol* 3:349–363.
13. Gunst SJ, Zhang W (2008) Actin cytoskeletal dynamics in smooth muscle: A new paradigm for the regulation of smooth muscle contraction. *Am J Physiol Cell Physiol* 295:C576–C587.
14. Humphrey JD, Schwartz MA, Tellides G, Milewicz DM (2015) Role of mechanotransduction in vascular biology: Focus on thoracic aortic aneurysms and dissections. *Circ Res* 116:1448–1461.
15. Milewicz DM, et al. (2017) Altered smooth muscle cell force generation as a driver of thoracic aortic aneurysms and dissections. *Arterioscler Thromb Vasc Biol* 37:26–34.
16. Guo D-C, et al. (2009) Mutations in smooth muscle alpha-actin (ACTA2) cause coronary artery disease, stroke, and Moyamoya disease, along with thoracic aortic disease. *Am J Hum Genet* 84:617–627.
17. Lu H, Fagnant PM, Bookwalter CS, Joel P, Trybus KM (2015) Vascular disease-causing mutation R258C in ACTA2 disrupts actin dynamics and interaction with myosin. *Proc Natl Acad Sci USA* 112:E4168–E4177.
18. Strauch AR, Rubenstein PA (1984) A vascular smooth muscle alpha-isoactin biosynthetic intermediate in BC3H1 cells. Identification of acetylcysteine at the NH2 terminus. *J Biol Chem* 259:7224–7229.
19. Malloy LE, et al. (2012) Thoracic aortic aneurysm (TAAD)-causing mutation in actin affects formin regulation of polymerization. *J Biol Chem* 287:28398–28408.
20. Rubenstein PA, Wen KK (2014) Insights into the effects of disease-causing mutations in human actins. *Cytoskeleton* 71:211–229.
21. Velasquez LS, et al. (2013) Activation of MRTF-A-dependent gene expression with a small molecule promotes myofibroblast differentiation and wound healing. *Proc Natl Acad Sci USA* 110:16850–16855.
22. Allsopp RC, et al. (1992) Telomere length predicts replicative capacity of human fibroblasts. *Proc Natl Acad Sci USA* 89:10114–10118.
23. Cristofalo VJ, Allen RG, Pignolo RJ, Martin BG, Beck JC (1998) Relationship between donor age and the replicative lifespan of human cells in culture: A reevaluation. *Proc Natl Acad Sci USA* 95:10614–10619.
24. Small EM, et al. (2010) Myocardin-related transcription factor-a controls myofibroblast activation and fibrosis in response to myocardial infarction. *Circ Res* 107: 294–304.
25. Crider BJ, Risinger GM, Jr, Haaksma CJ, Howard EW, Tomasek JJ (2011) Myocardin-related transcription factors A and B are key regulators of TGF-β1-induced fibroblast to myofibroblast differentiation. *J Invest Dermatol* 131:2378–2385.
26. Desmoulière A, Geinoz A, Gabbiani F, Gabbiani G (1993) Transforming growth factor-beta 1 induces alpha-smooth muscle actin expression in granulation tissue myofibroblasts and in quiescent and growing cultured fibroblasts. *J Cell Biol* 122:103–111.
27. Grinnell F, Petroll WM (2010) Cell motility and mechanics in three-dimensional collagen matrices. *Annu Rev Cell Dev Biol* 26:335–361.
28. Ouellette MM, McDaniel LD, Wright WE, Shay JW, Schultz RA (2000) The establishment of telomerase-immortalized cell lines representing human chromosome instability syndromes. *Hum Mol Genet* 9:403–411.
29. Walter M, Forsyth NR, Wright WE, Shay JW, Roth MG (2004) The establishment of telomerase-immortalized Tangier disease cell lines indicates the existence of an apolipoprotein A-I-inducible but ABCA1-independent cholesterol efflux pathway. *J Biol Chem* 279:20866–20873.
30. Papke CL, et al. (2013) Smooth muscle hyperplasia due to loss of smooth muscle α-actin is driven by activation of focal adhesion kinase, altered p53 localization and increased levels of platelet-derived growth factor receptor-β. *Hum Mol Genet* 22: 3123–3137.
31. Chen L, et al. (2016) Smooth muscle-alpha actin inhibits vascular smooth muscle cell proliferation and migration by inhibiting Rac1 activity. *PLoS One* 11:e0155726.
32. Wang J, Zohar R, McCulloch CA (2006) Multiple roles of alpha-smooth muscle actin in mechanotransduction. *Exp Cell Res* 312:205–214.
33. Hinz B, et al. (2012) Recent developments in myofibroblast biology: Paradigms for connective tissue remodeling. *Am J Pathol* 180:1340–1355.
34. Olson EN, Nordheim A (2010) Linking actin dynamics and gene transcription to drive cellular motile functions. *Nat Rev Mol Cell Biol* 11:353–365.
35. Dugina V, Alexandrova A, Chaponnier C, Vasiliev J, Gabbiani G (1998) Rat fibroblasts cultured from various organs exhibit differences in alpha-smooth muscle actin expression, cytoskeletal pattern, and adhesive structure organization. *Exp Cell Res* 238: 481–490.
36. Chen CS, Alonso JL, Ostuni E, Whitesides GM, Ingber DE (2003) Cell shape provides global control of focal adhesion assembly. *Biochem Biophys Res Commun* 307: 355–361.
37. Elosegui-Artola A, et al. (2014) Image analysis for the quantitative comparison of stress fibers and focal adhesions. *PLoS One* 9:e107393.
38. Hinz B, Dugina V, Ballestrem C, Wehrle-Haller B, Chaponnier C (2003) Alpha-smooth muscle actin is crucial for focal adhesion maturation in myofibroblasts. *Mol Biol Cell* 14:2508–2519.
39. Clément S, Hinz B, Dugina V, Gabbiani G, Chaponnier C (2005) The N-terminal Ac-EEED sequence plays a role in alpha-smooth-muscle actin incorporation into stress fibers. *J Cell Sci* 118:1395–1404.
40. Hinz B, Celetta G, Tomasek JJ, Gabbiani G, Chaponnier C (2001) Alpha-smooth muscle actin expression upregulates fibroblast contractile activity. *Mol Biol Cell* 12: 2730–2741.
41. Dugina V, Fontao L, Chaponnier C, Vasiliev J, Gabbiani G (2001) Focal adhesion features during myofibroblastic differentiation are controlled by intracellular and extracellular factors. *J Cell Sci* 114:3285–3296.
42. Rønnov-Jessen L, Petersen OW (1996) A function for filamentous alpha-smooth muscle actin: Retardation of motility in fibroblasts. *J Cell Biol* 134:67–80.
43. Sapudom J, et al. (2015) The interplay of fibronectin functionalization and TGF-β1 presence on fibroblast proliferation, differentiation and migration in 3D matrices. *Biomater Sci* 3:1291–1301.
44. Bell E, Ivarsson B, Merrill C (1979) Production of a tissue-like structure by contraction of collagen lattices by human fibroblasts of different proliferative potential in vitro. *Proc Natl Acad Sci USA* 76:1274–1278.
45. Guidry C, Grinnell F (1985) Studies on the mechanism of hydrated collagen gel reorganization by human skin fibroblasts. *J Cell Sci* 79:67–81.
46. Kasugai S, Ogura H (1993) The effects of cytoskeletal inhibitors on the collagen gel contraction by dog periodontal ligament fibroblasts in vitro. *Arch Oral Biol* 38: 785–792.
47. Arora PD, McCulloch CA (1994) Dependence of collagen remodelling on alpha-smooth muscle actin expression by fibroblasts. *J Cell Physiol* 159:161–175.
48. Gao N, et al. (2013) Signaling through myosin light chain kinase in smooth muscles. *J Biol Chem* 288:7596–7605.
49. Milewicz DM, et al. (2010) De novo ACTA2 mutation causes a novel syndrome of multisystemic smooth muscle dysfunction. *Am J Med Genet A* 152A:2437–2443.
50. Lu H, Fagnant PM, Krementsova EB, Trybus KM (2016) Severe molecular defects exhibited by the R179H mutation in human vascular smooth muscle α-actin. *J Biol Chem* 291:21729–21739.
51. Ouellette MM, Aisner DL, Savre-Train I, Wright WE, Shay JW (1999) Telomerase activity does not always imply telomere maintenance. *Biochem Biophys Res Commun* 254:795–803.
52. Kulak O, et al. (2015) Disruption of Wnt/β-catenin signaling and telomeric shortening are inextricable consequences of tankyrase inhibition in human cells. *Mol Cell Biol* 35: 2425–2435.
53. Ludlow AT, et al. (2014) Quantitative telomerase enzyme activity determination using droplet digital PCR with single cell resolution. *Nucleic Acids Res* 42:e104.
54. da Rocha-Azevedo B, Ho CH, Grinnell F (2013) Fibroblast cluster formation on 3D collagen matrices requires cell contraction dependent fibronectin matrix organization. *Exp Cell Res* 319:546–555.
55. Liu Z, Ho CH, Grinnell F (2014) The different roles of myosin IIA and myosin IIB in contraction of 3D collagen matrices by human fibroblasts. *Exp Cell Res* 326:295–306.
56. Berginski ME, Vitriol EA, Hahn KM, Gomez SM (2011) High-resolution quantification of focal adhesion spatiotemporal dynamics in living cells. *PLoS One* 6:e22025.
57. Berginski ME, Gomez SM (2013) The Focal Adhesion Analysis Server: A web tool for analyzing focal adhesion dynamics. *F1000 Res* 2:68.
58. Grinnell F (2000) Fibroblast-collagen-matrix contraction: Growth-factor signalling and mechanical loading. *Trends Cell Biol* 10:362–365.